Instrumentation to rapidly acquire fluorescence wavelength-time matrices of biological tissues

William R. Lloyd,[1] Robert H. Wilson,[2] Ching-Wei Chang,[1] Gregory D. Gillispie,[3] and Mary-Ann Mycek[1, 2, *]

[1]*Department of Biomedical Engineering, University of Michigan, Ann Arbor, MI 48109-2099, USA*
[2]*Applied Physics Program, University of Michigan, Ann Arbor, MI 48109-0362, USA*
[3]*Fluorescence Innovations, Inc., Bozeman, MT 59718, USA*
**mycek@umich.edu*

Abstract: A fiber-optic system was developed to rapidly acquire tissue fluorescence wavelength-time matrices (WTMs) with high signal-to-noise ratio (SNR). The essential system components (473 nm microchip laser operating at 3 kHz repetition frequency, fiber-probe assemblies, emission monochromator, photomultiplier tube, and digitizer) were assembled into a compact and clinically-compatible unit. Data were acquired from fluorescence standards and tissue-simulating phantoms to test system performance. Fluorescence decay waveforms with SNR > 100 at the decay curve peak were obtained in less than 30 ms. With optimized data transfer and monochromator stepping functions, it should be feasible to acquire a full WTM at 5 nm emission wavelength intervals over a 200 nm range in under 2 seconds.

©2010 Optical Society of America

OCIS codes: (170.6510) Spectroscopy, tissue diagnostics; (170.3650) Lifetime-based sensing

References and links

1. M. A. Mycek, and B. W. Pogue, eds., *Handbook of Biomedical Fluorescence* (Marcel-Dekker Inc., New York, New York, 2003).
2. J. D. Pitts, and M.-A. Mycek, "Design and development of a rapid acquisition laser-based fluorometer with simultaneous spectral and temporal resolution," Rev. Sci. Instrum. **72**(7), 3061–3072 (2001).
3. Q. Fang, T. Papaioannou, J. A. Jo, R. Vaitha, K. Shastry, and L. Marcu, "Time-domain laser-induced fluorescence spectroscopy apparatus for clinical diagnostics," Rev. Sci. Instrum. **75**(1), 151–162 (2004).
4. M. Chandra, K. Vishwanath, G. D. Fichter, E. Liao, S. J. Hollister, and M.-A. Mycek, "Quantitative molecular sensing in biological tissues: an approach to non-invasive optical characterization," Opt. Express **14**(13), 6157–6171 (2006).
5. Z. Volynskaya, A. S. Haka, K. L. Bechtel, M. Fitzmaurice, R. Shenk, N. Wang, J. Nazemi, R. R. Dasari, and M. S. Feld, "Diagnosing breast cancer using diffuse reflectance spectroscopy and intrinsic fluorescence spectroscopy," J. Biomed. Opt. **13**(2), 024012 (2008).
6. S. K. Chang, N. Marin, M. Follen, and R. Richards-Kortum, "Model-based analysis of clinical fluorescence spectroscopy for *in vivo* detection of cervical intraepithelial dysplasia," J. Biomed. Opt. **11**(2), 024008 (2006).
7. I. Georgakoudi, and M. S. Feld, "The combined use of fluorescence, reflectance, and light-scattering spectroscopy for evaluating dysplasia in Barrett's esophagus," Gastrointest. Endosc. Clin. N. Am. **14**(3), 519–537, ix (2004).
8. T. J. Pfefer, D. Y. Paithankar, J. M. Poneros, K. T. Schomacker, and N. S. Nishioka, "Temporally and spectrally resolved fluorescence spectroscopy for the detection of high grade dysplasia in Barrett's esophagus," Lasers Surg. Med. **32**(1), 10–16 (2003).
9. Y. S. Fawzy, and H. Zeng, "Intrinsic fluorescence spectroscopy for endoscopic detection and localization of the endobronchial cancerous lesions," J. Biomed. Opt. **13**(6), 064022 (2008).
10. M. Chandra, J. Scheiman, D. Heidt, D. Simeone, B. McKenna, and M.-A. Mycek, "Probing pancreatic disease using tissue optical spectroscopy," J. Biomed. Opt. **12**(6), 060501 (2007).
11. R. H. Wilson, M. Chandra, J. Scheiman, D. Simeone, B. McKenna, J. Purdy, and M. A. Mycek, "Optical spectroscopy detects histological hallmarks of pancreatic cancer," Opt. Express **17**(20), 17502–17516 (2009).
12. M. Chandra, J. Scheiman, D. Simeone, B. McKenna, J. Purdy, and M.-A. Mycek, "Spectral areas and ratios classifier algorithm for pancreatic tissue classification using optical spectroscopy," J. Biomed. Opt. **15**(1), 010514 (2010).

#130228 - $15.00 USD Received 16 Jun 2010; revised 6 Aug 2010; accepted 7 Aug 2010; published 10 Aug 2010
(C) 2010 OSA

13. W. H. Yong, P. V. Butte, B. K. Pikul, J. A. Jo, Q. Y. Fang, T. Papaioannou, K. Black, and L. Marcu, "Distinction of brain tissue, low grade and high grade glioma with time-resolved fluorescence spectroscopy," Front. Biosci. **11**(1), 1255–1263 (2006).
14. L. Marcu, J. A. Jo, P. V. Butte, W. H. Yong, B. K. Pikul, K. L. Black, and R. C. Thompson, "Fluorescence lifetime spectroscopy of glioblastoma multiforme," Photochem. Photobiol. **80**(1), 98–103 (2004).
15. M.-A. Mycek, K. T. Schomacker, and N. S. Nishioka, "Colonic polyp differentiation using time-resolved autofluorescence spectroscopy," Gastrointest. Endosc. **48**(4), 390–394 (1998).
16. K. Vishwanath, and M.-A. Mycek, "Do fluorescence decays remitted from tissues accurately reflect intrinsic fluorophore lifetimes?" Opt. Lett. **29**(13), 1512–1514 (2004).
17. P. Uehlinger, T. Gabrecht, T. Glanzmann, J.-P. Ballini, A. Radu, S. Andrejevic, P. Monnier, and G. Wagnières, "*In vivo* time-resolved spectroscopy of the human bronchial early cancer autofluorescence," J. Biomed. Opt. **14**(2), 024011 (2009).
18. N. Lois, and J. V. Forrester, *Fundus Autofluorescence* (Lippincott Williams & Wilkins, Philadelphia, 2009).
19. F. G. Holz, and R. F. Spaide, *Medical Retina: Focus on Retinal Imaging* (Springer-Verlag, Berlin, 2010).
20. L. Marcu, "Fluorescence lifetime in cardiovascular diagnostics," J. Biomed. Opt. **15**(1), 011106 (2010).
21. J. Blackwell, K. M. Katika, L. Pilon, K. M. Dipple, S. R. Levin, and A. Nouvong, "*In vivo* time-resolved autofluorescence measurements to test for glycation of human skin," J. Biomed. Opt. **13**(1), 014004 (2008).
22. J. R. Lakowicz, *Principles of Fluorescence Spectroscopy* (Kluwer Academic/Plenum, New York, 1999).
23. K. Vishwanath, W. Zhong, M. Close, and M.-A. Mycek, "Fluorescence quenching by polystyrene microspheres in UV-visible and NIR tissue-simulating phantoms," Opt. Express **14**(17), 7776–7788 (2006).
24. A. J. Bystol, T. Thorstenson, and A. D. Campiglia, "Laser-induced multidimensional fluorescence spectroscopy in Shpol'skii matrixes for the analysis of polycyclic aromatic hydrocarbons in HPLC fractions and complex environmental extracts," Environ. Sci. Technol. **36**(20), 4424–4429 (2002).
25. A. J. Bystol, A. D. Campiglia, and G. D. Gillispie, "Laser-induced multidimensional fluorescence spectroscopy in Shpol'skii matrixes with a fiber-optic probe at liquid helium temperature," Anal. Chem. **73**(23), 5762–5770 (2001).
26. A. J. Bystol, A. D. Campiglia, and G. D. Gillispie, "Time-resolved laser-excited Shpol'skii spectrometry with a fiber-optic probe and ICCD camera," Appl. Spectrosc. **54**(6), 910–917 (2000).
27. R. Mekhala, D. S. Nadder, H. W. Robert, M. Mary-Ann, P. Nancy, H. K. David, and D. M. Michael, "Quantitative polarized Raman spectroscopy in highly turbid bone tissue," J. Biomed. Opt. **15**, 037001 (2010).
28. S. A. Prahl, M. J. C. van Gemert, and A. J. Welch, "Determining the optical properties of turbid media by using the adding-doubling method," Appl. Opt. **32**(4), 559–568 (1993).
29. D. Hai, F. Ru-Chun Amy, L. Junzhong, L. A. Corkan, and S. L. Jonathan, "PhotochemCAD: A Computer-Aided Design and Research Tool in Photochemistry," Photochem. Photobiol. **68**, 141–142 (1998).
30. D. Magde, G. E. Rojas, and P. G. Seybold, "Solvent dependence of the fluorescence lifetimes of xanthene dyes," Photochem. Photobiol. **70**(5), 737–744 (1999).
31. K. Vishwanath, B. W. Pogue, and M.-A. Mycek, "Quantitative fluorescence lifetime spectroscopy in turbid media: comparison of theoretical, experimental and computational methods," Phys. Med. Biol. **47**(18), 3387–3405 (2002).
32. K. Vishwanath, and M.-A. Mycek, "Time-resolved photon migration in bi-layered tissue models," Opt. Express **13**(19), 7466–7482 (2005).

1. Introduction

The multidimensional data provided by fluorescence spectroscopy opens up the possibility of rapidly deriving quantitative diagnostic information from tissues in a minimally-invasive manner [1]. Steady-state and time-resolved fluorescence measurements have been performed with instrumentation designed for eventual translation to the clinic [2–4]. Steady-state fluorescence spectroscopy has been employed for cancer diagnostics in organs including the breast [5], cervix [6], esophagus [7,8], lung [9], and pancreas [10–12]. Time-resolved fluorescence spectroscopy has been employed for cancer diagnostics in organs including the brain [13,14], colon [15,16], esophagus [8], and lung [17]. Steady-state and time-resolved fluorescence measurements have been employed in ophthalmology for detection of conditions including macular degeneration, diabetic retinopathy, and retinal artery occlusion [18,19]. Time-resolved fluorescence measurements have also recently been used for the detection of cardiovascular disease [20] and type 2 diabetes [21].

Although steady-state fluorescence can reveal information about fluorophores in a biological tissue, the intensity of steady-state spectra are influenced by a variety of artifacts [3]. Time-resolved fluorescence measurements provide the fluorescence lifetime τ, which is the mean time spent by a fluorophore in its excited state [22]. The lifetime value is sensitive to the environment of the fluorophore, so it can vary with changes in binding, pH, oxygen,

#130228 - $15.00 USD Received 16 Jun 2010; revised 6 Aug 2010; accepted 7 Aug 2010; published 10 Aug 2010
(C) 2010 OSA

and temperature. Importantly, lifetime measurements are not strongly dependent on intensity-based effects such as absorption, photobleaching, and changes in excitation intensity and collection efficiency [3,23]. Lifetime values for multiple fluorophores in a sample can be obtained from time-resolved fluorescence measurements, even if the steady-state spectra of the fluorophores overlap. Therefore, steady-state and time-resolved methods are both useful tools for characterization of biological tissue fluorescence.

Ideally one would maximize the amount of independent fluorescence information and the quality of the data (signal-to-noise ratio, for example) for every sample. However, clinical applications require consideration of measurement speed, portability, cost, and ease of use. The first *in vivo* endoscopic time-resolved fluorescence measurements on human patients were reported in 1998, using a portable, fiber-optic based system with a low repetition-rate laser and limited spectral resolution [15,16]. Since then, two strategies have been employed for combining spectral and temporal fluorescence data collection in a clinically compatible format. The first approach uses one laser excitation source, but two different detection platforms. The spectral and temporal data are collected in sequence, but could be obtained simultaneously. The second approach collects a full fluorescence wavelength-time matrix (WTM, Fig. 1) by stepping an emission monochromator through a series of wavelengths, such that a fluorescence decay curve is produced sequentially at each of those wavelengths. Integrating the WTM over time yields a steady-state fluorescence spectrum. Integrating the WTM over wavelength yields a time-resolved fluorescence decay curve.

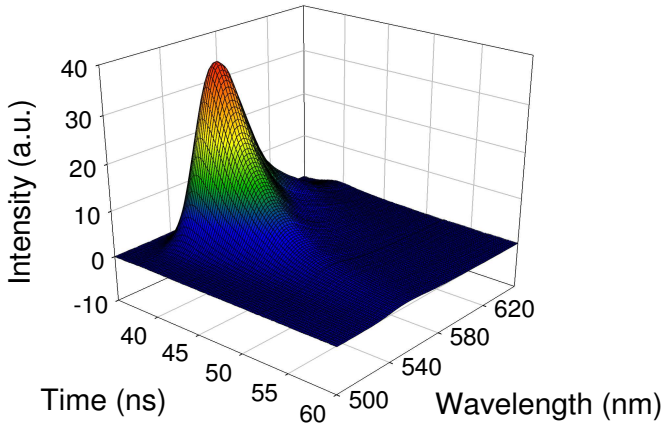

Fig. 1. Fluorescence wavelength-time matrix (WTM) of 1 μM Rhodamine 6G in ethanol acquired with fiber-optic probes for light delivery and detection. The WTM contains both wavelength-resolved and time-resolved fluorescence data.

In this study, a specialized compact digitizer was employed to obtain WTMs from samples excited with a microchip laser, which had a repetition rate significantly higher than that used in similar spectroscopic devices [8,14,15,20]. Section 2 describes the technology developed for detecting fluorescence WTMs, the incorporation of this technology into a clinically compatible fiber-probe based instrument, and the experimental methods employed to assess the technology. Section 3 details system characterization using standard fluorophore solutions. Section 4 describes using the system to acquire fluorescence WTMs from tissue-simulating phantoms.

2. Instrumentation and experimental methods

2.1 Clinically-compatible instrumentation

The instrumentation (Fig. 2) consisted of a 473 nm microchip laser (Lumanova, 20-030005, μFlare Blue, 3 kHz pulse repetition rate, ~2 ns pulse duration), a specialized transient digitizer

#130228 - $15.00 USD Received 16 Jun 2010; revised 6 Aug 2010; accepted 7 Aug 2010; published 10 Aug 2010
(C) 2010 OSA

(Fluorescence Innovations (FI), Inc., Bozeman, MT) for WTM measurement [24–26], a scanning monochromator (Optometrics, MC1-03), and a photo-multiplier tube (PMT) (Hamamatsu, H6780-20).

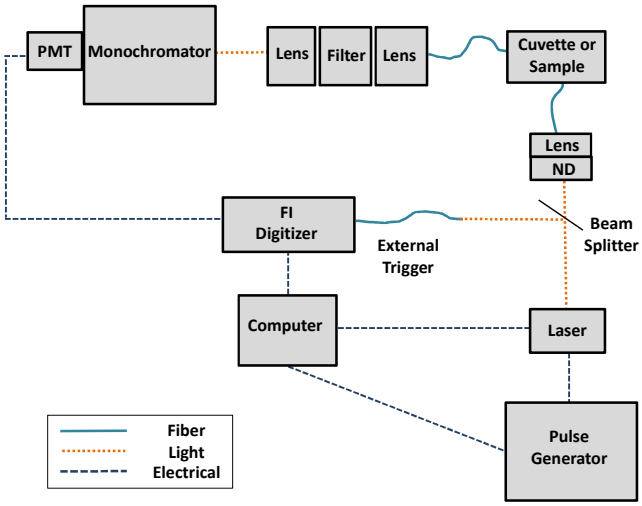

Fig. 2. Schematic of the instrumentation developed for rapid acquisition of fluorescence WTMs, using fiber-optic probes for light delivery and detection (set-up 4, Table 1). WTMs were also obtained with three other set-ups (Table 1): (1) right-angle free-space geometry, in place of the fiber-probes, for light delivery and detection; (2) free-space light delivery and a fiber-probe for fluorescence detection; (3) a fiber-probe for light delivery and right-angle free-space geometry for detection.

The FI digitizer is an extremely compact, low power digitizer for direct waveform recording of the fluorescence decay curves. Its unique 10-bit, fast-in slow-out, analog-to-digital converter operates at 1 gigasample/second (GS/s) with a sampling depth of 128 ns. For most applications, 5X interleaving is applied to increase the effective sampling rate to 5 GS/s. This approach permits high-speed sampling without requiring equally high-speed conversion, which enables very reliable digitization. Event rates in excess of 25 kHz are possible. A graphical user interface enables user control over input parameters.

The digitizer can be employed to measure single-laser pulse collections. Additional laser pulses can be averaged to increase the signal-to-noise ratio. The time increase for measurements with additional laser pulses averaged is proportional to the increased number of laser pulses, with a small increase in pulses averaged not greatly affecting total collection time due to the rapid acquisition speed and high repetition rate laser employed. For samples with a lower concentration of fluorophores and weaker fluorescence signal, the PMT voltage can be increased prior to measurement to maximize the dynamic range of the digitizer. The detection system has a wavelength resolution of 0.01 nm and a temporal resolution of 200 ps.

The dimensions of the main system components are: 16 cm x 10.3 cm x 3.0 cm (digitizer), 9.5 cm x 4.0 cm x 7.0 cm (microchip laser), 15.2 cm x 6.4 cm x 6.4 cm (monochromator), 5.1 cm x 2.6 cm x 2.6 cm (PMT), 19.5 cm x 5 cm x 10 cm (laser power supply), and 16.5 cm x 10.5 cm x 4.5 cm (pulse generator). This small table-top footprint makes the system ideal for eventual translation to a clinical setting.

2.2 Optical configurations (fiber optics vs. free space)

For system characterization, four different system set-ups (Table 1) were employed to acquire WTMs from standard fluorophore solutions. Set-up 1 was a free-space right-angle geometry commonly used for cuvette-based measurements. Set-ups 2 and 3 were identical to set-up 1, except that set-up 2 used a fiber for detection and set-up 3 used a fiber for light delivery. Set-

#130228 - $15.00 USD Received 16 Jun 2010; revised 6 Aug 2010; accepted 7 Aug 2010; published 10 Aug 2010
(C) 2010 OSA

up 4 (Fig. 2) was clinically compatible because it used fiber-optic probes (Fiberguide Industries, SFS600/660N, 600 μm core diameter) for light delivery and detection. For the reported studies, fiber-optic probes were inserted vertically 1 cm below the top surface of the fluorophore solution and 3 cm above the bottom of the cuvette with a 660 μm probe spacing.

Table 1. Set-ups employed to acquire fluorescence WTMs

Set-up	Light delivery	Fluorescence detection
1	Direct illumination	Right-angle detection
2	Direct illumination	Fiber-optic probe
3	Fiber-optic probe	Right-angle detection
4	Fiber-optic probe	Fiber-optic probe

Focusing lenses (Thorlabs, LA4306-UV, LA4052-UV) and a 500 nm longpass filter (Semrock, FF01-488) were employed in set-ups 2 and 4 to couple and filter light from the fiber-optic probe to the monochromator. In set-up 4, fiber holders were attached to micrometer stages for controlled source-detector spacing.

2.3 Sample preparation

2.3.1 Standard fluorophore solutions

The system performance was tested (Section 3) by acquiring WTMs from solutions of three standard fluorophores: rhodamine 6G (Sigma, R4127), fluorescein (Sigma, 166308), and rose bengal (Sigma, 330000). Each fluorophore was made with a 1 μM concentration in ethanol. The solutions were thoroughly mixed in a cuvette prior to measurement. Signal-to-noise characterization of the system was performed with a stock solution (~1.7×10^7 beads/mL) of fluorescent beads (Invitrogen, A7303).

2.3.2 Tissue-simulating phantoms

Four tissue-simulating phantoms were made with different scattering coefficients. Each phantom originated from a ~1 mM solution of Rhodamine B (Sigma, R6626) in deionized water. For the first phantom, 4 mL of deionized water was combined with 4 μL of the original Rhodamine B solution. For the second phantom, 3.5 mL of deionized water was combined with 0.5 mL polystyrene microspheres (Duke Standards, 4009A, 1μm diameter) before adding 4 μL of the Rhodamine B solution. For the third phantom, 3 mL of deionized water was combined with 1 mL of polystyrene microspheres before adding 4 μL of the Rhodamine B solution. The fourth phantom was made by combining 2 mL of deionized water with 2 mL of the polystyrene microspheres before adding 4 μL of the Rhodamine B solution. Thus, the resulting concentration of Rhodamine B in each mixture was 1 μM. Each of these mixtures was then thoroughly combined with ~0.025 g of powder gelatin (Sigma, 097K0108) in a 50 mL conical tube. Then, each mixture was transferred to a 35 mm Petri dish and placed on an 80°C hot plate for 20 minutes to dissolve the gelatin, stirring every 5 minutes. Each sample was removed from the hot plate and returned to room temperature before refrigeration at 3°C overnight to solidify the sample. The resulting thickness of each phantom was ~4 mm.

An integrating sphere (RT-060-SF, Labsphere, North Sutton, NH) set-up was employed to measure the scattering coefficient for each phantom [27]. Briefly, a lamp with a Kohler illuminator (KI-120, Labsphere) was connected to a power supply (LPS-150-0660, Labsphere) to uniformly illuminate each phantom. Two configurations, one for reflectance and one for transmittance, were used; in both cases, the detected light traveled from the integrating sphere into a spectrometer (Ocean Optics, Dunedin, FL, HR2000 +) via an optical fiber (Ocean Optics, P1000-2-VIS-NIR). The wavelength-resolved reflectance and transmittance of each phantom were input into an inverse adding-doubling (IAD) algorithm [28] to obtain the absorption and scattering coefficients. For the four phantoms, three of

#130228 - $15.00 USD Received 16 Jun 2010; revised 6 Aug 2010; accepted 7 Aug 2010; published 10 Aug 2010
(C) 2010 OSA

which contained microspheres, the IAD algorithm extracted negligible absorption coefficients and scattering coefficients of 10 cm^{-1}, 50 cm^{-1}, 108 cm^{-1}, and 222 cm^{-1}.

3. System characterization - reference fluorophores in fluid solution

3.1. Signal-to-noise as function of acquisition time

A stock solution of fluorescent beads was used to measure the signal-to-noise ratio of the system as a function of laser pulses averaged per waveform (Fig. 3). Fluorescence decays were collected at 550 nm only and the standard deviation of fluorescence intensity from ten measurements was calculated by averaging standard deviations of intensity around the emission decay maximum (t = 36–38 ns). In Fig. 3(a), the standard deviations (green curve) were measured with system set-up 4 (Fig. 2) and were obtained for acquisition times corresponding to 5, 125, 250, 375, 500, 750, 1000, 1250, and 1500 laser pulses averaged. The result was characteristic of Poisson noise (blue curve), which was defined as the square root of mean intensity divided by the square root of the number of laser pulses averaged, and multiplied by a factor of 0.045 to match the scale of the experimental results. The arrow in Fig. 3(a) represents fluorescence acquisition with 125 laser pulses averaged. This fluorescence detection had a peak intensity of ~28 (a.u.) and a standard deviation of ~0.25 (a.u.), yielding a SNR greater than 100.

Figure 3(b) shows two measurements of time-resolved fluorescence: one obtained with 5 laser pulses (red curve), and the other obtained with 1250 pulses (purple curve). These two curves correspond to the circled collection points in Fig. 5(a). The two curves were similar in shape despite a 250-fold decrease in the number of laser pulses averaged.

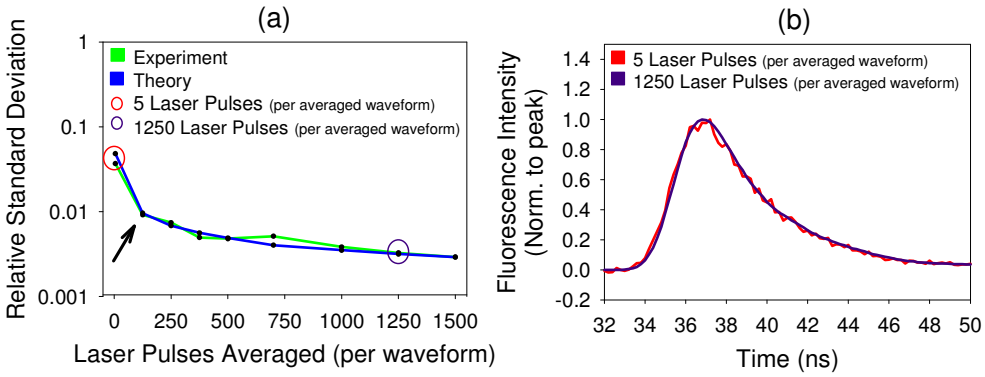

Fig. 3. Signal-to-noise characterization of the system, performed on a stock solution of fluorescent beads: (a) standard deviation of measured fluorescence intensity (green curve), compared to prediction of Poisson theory (blue curve), as a function of acquisition time; (b) normalized fluorescence decay curves for 5 laser pulses averaged (red curve, corresponding to red circle in (a)) and 1250 laser pulses averaged (purple curve, corresponding to purple circle in (a)). The arrow in (a) denotes data acquisition with 125 laser pulses averaged; the standard deviation of the relative peak intensity at this point is ~0.25 (a.u.) with a peak signal intensity of ~28 (a.u.), yielding a SNR greater than 100.

3.2 Wavelength-resolved fluorescence

WTMs were acquired from the standard fluorophore solutions from 500 to 650 nm in steps of 2 nm, using 1250 laser pulses for excitation per wavelength. Time-resolved fluorescence was acquired from 0 to 127.8 ns in steps of 0.2 ns. The PMT setting was varied to keep detected signal within the operating range of the digitizer. Prior to data acquisition, the emission intensity of each sample was monitored for one minute to verify that no photobleaching occurred.

#130228 - $15.00 USD Received 16 Jun 2010; revised 6 Aug 2010; accepted 7 Aug 2010; published 10 Aug 2010
(C) 2010 OSA

Figure 4 shows the time-integrated fluorescence spectrum of each standard fluorophore solution. For each fluorophore, three measurements with the fiber-based set-up (set-up 4, Fig. 2) were averaged to obtain the spectra shown in Fig. 4. The error bars (standard deviation) were similar in size for all four of the system set-ups (data not shown). The collection time for each WTM was 82 seconds. The wavelength range measured was 500 to 650 nm with a 2 nm step size. For each wavelength, 1250 laser pulses were averaged to produce the time-resolved decay. These data were in good qualitative agreement (peak intensity wavelength agreed within 2 nm) with those reported in the literature [29].

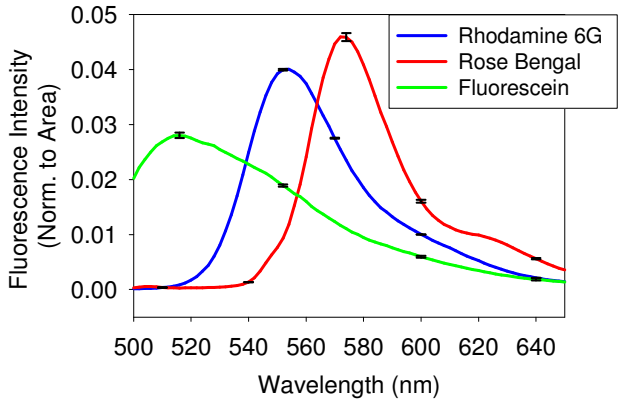

Fig. 4. Fluorescence spectra of rhodamine 6G (blue curve), rose bengal (red curve), and fluorescein (green curve), measured with the fiber-based system set-up 4 and normalized to the area under the curve. Each curve is the average of three measurements; the error bars represent the standard deviation.

3.3 Time-resolved fluorescence and extraction of fluorescence lifetimes

Figure 5 shows time-resolved fluorescence decay curves obtained with the four system set-ups for rhodamine 6G [Fig. 5(a)], rose bengal [Fig. 5(b)], and fluorescein [Fig. 5(c)]. Each plot represents the average of the time-resolved fluorescence decays acquired for four set-ups (Fig. 2) and multiple emission wavelengths. For each of these three plots, time-resolved measurements at the peak emission wavelength as well as wavelengths corresponding to 0.6x peak intensity were averaged. Time-resolved fluorescence was obtained at three different emission wavelengths for rhodamine 6G and rose bengal. Time-resolved fluorescence from fluorescein was obtained at only two different emission wavelengths because the emission peak of fluorescein was near the first collection wavelength. The time-resolved fluorescence decays for each set-up were shifted to a common peak value for comparison, because integrating fiber-optic probes into the system set-ups changed the travel time slightly for delivered laser pulses and detected fluorescence. The error bars plot the standard deviation for each fluorophore, indicating that the measured time-resolved decays are consistent across collection wavelengths and system set-up geometries.

#130228 - $15.00 USD Received 16 Jun 2010; revised 6 Aug 2010; accepted 7 Aug 2010; published 10 Aug 2010
(C) 2010 OSA

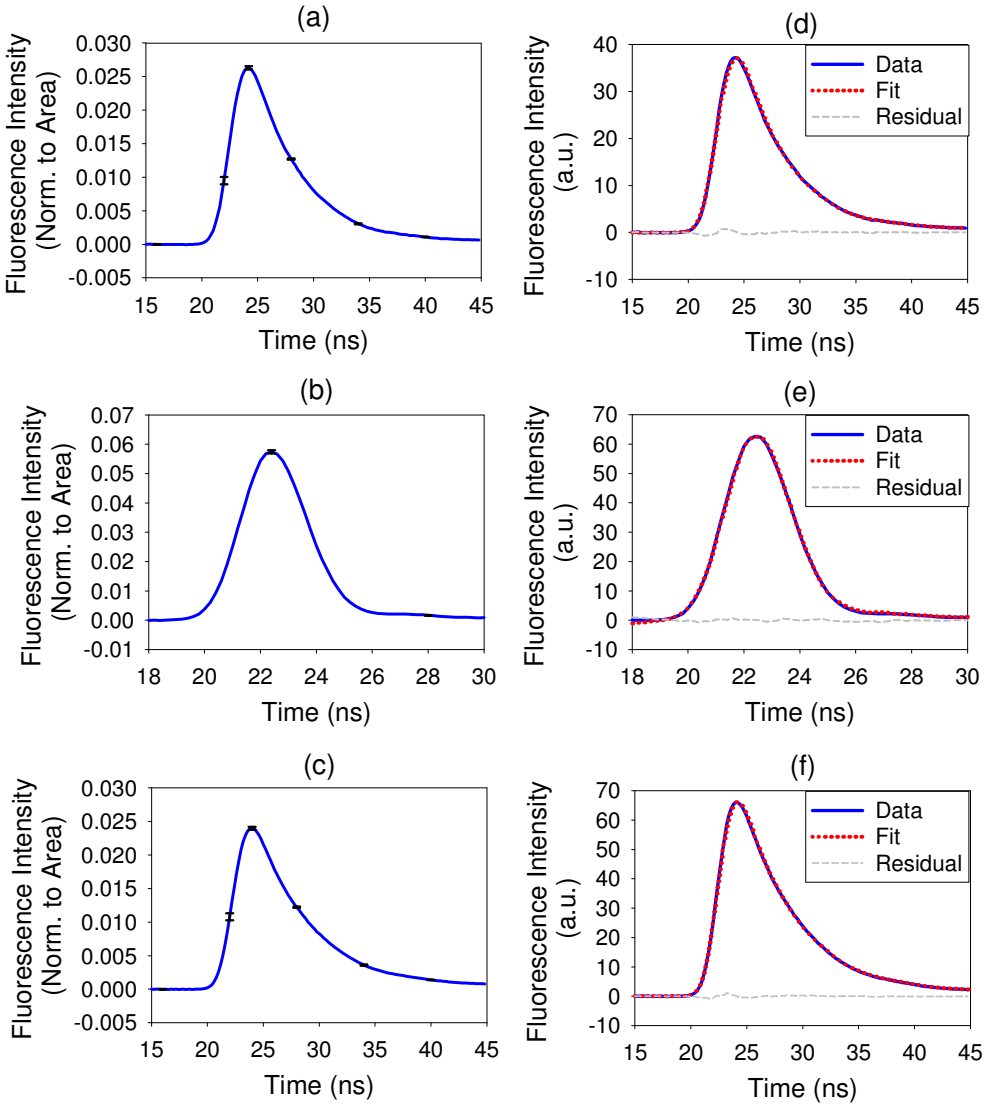

Fig. 5. Time-resolved fluorescence decay curves measured on solutions of rhodamine 6G ((a), (d)), rose bengal ((b), (e)), and fluorescein ((c), (f)). Panel (a) plots 36 averaged rhodamine 6G fluorescence decays, panel (b) plots 36 averaged rose bengal fluorescence decays, and panel (c) plots 24 averaged fluorescein fluorescence decays (four system set-ups per fluorophore, three emission wavelengths for rhodamine 6G and rose bengal, two emission wavelengths for fluorescein). The error bars represent standard deviation. In panels (d), (e), and (f), one representative decay curve for each fluorophore measured with set-up 4 was fit to a single exponential decay.

Figure 5 also shows fits of representative time-resolved fluorescence curves measured with set-up 4 from rhodamine 6G [Fig. 5(d)], rose bengal [Fig. 5(e)], and fluorescein [Fig. 5(f)] to a single-exponential decay $e^{-t/\tau}$, where τ is the mean fluorophore lifetime. An iterative least-squares fitting algorithm was employed to obtain these fits and extract the corresponding lifetime values [25]. In order to perform the fitting procedure, the instrument response function (IRF) was also acquired for each detection setting. The IRF was measured from a sample of deionized water in a cuvette, using neutral density filters to reduce the transmitted light energy to the sample. All data was fit using an IRF taken within 1 nm of the

#130228 - $15.00 USD Received 16 Jun 2010; revised 6 Aug 2010; accepted 7 Aug 2010; published 10 Aug 2010
(C) 2010 OSA

excitation laser wavelength (473 nm), selected because it is independent of the wavelength of the fit data and repeatable across experiments. The residuals are presented to show the quality of each fit.

Lifetime analysis was performed on the four set-ups at the peak fluorescence wavelength from each fluorophore, as presented in Table 2. All data was fit as a single exponential decay with Fluorescence Analysis Fitting Software (Fluorescence Innovations (FI), Inc., Bozeman, MT). The extracted lifetimes were in good agreement with previously reported values and this agreement was consistent for each set-up. For each system set-up, three measurements were collected for each fluorophore and independently fit. The reported lifetime is the average of the three measurements plus or minus the standard deviation.

We note that the small discrepancies between lifetimes extracted for the four set-ups, as well as between the measured and literature values, could be due to differences in the way that the IRF was acquired, external factors such as temperature and pH, or impurities in the fluorophore solutions. For the measurements reported here, each fluorophore was used directly from the manufacturer without further purification, and temperature and pH conditions were not monitored.

Table 2. Lifetime values obtained from standard fluorophore solutions

		Measured [a]				**Literature**
		Set-up 1	**Set-up 2**	**Set-up 3**	**Set-up 4**	
Emission Wavelength (nm)	Fluorophore	Lifetime (ns)	Lifetime (ns)	Lifetime (ns)	Lifetime (ns)	Lifetime (ns)
550	Rhodamine 6G	3.977 ± 0.001	3.828 ± 0.004	3.971 ± 0.004	3.910 ± 0.001	3.99 ± 0.01 [30]
514	Fluorescein	4.449 ± 0.004	4.603 ± 0.007	4.534 ± 0.002	4.620 ± 0.004	4.25 ± 0.01 [30]
572	Rose Bengal	0.668 ± 0.014	0.676 ± 0.006	0.648 ± 0.003	0.711 ± 0.001	0.850 ± 0.030 [22]

[a]For each system set-up, three measurements were independently fit. The reported lifetimes are average plus or minus the standard deviation of these three fits.

4. Tissue-simulating phantom study

System set-up 4 (Fig. 2) was employed to acquire WTMs from four tissue-simulating phantoms with different scattering coefficients in a range relevant to biological tissue. The measured scattering coefficients of the tissue-simulating phantoms (Section 2.3.2) were 10 cm^{-1}, 50 cm^{-1}, 108 cm^{-1}, and 222 cm^{-1}. A 0.66 mm fiber-probe source-detector separation was used during WTM collection for each phantom. Additional measurements with fiber-probe source-detector separations of 1.66 mm, 2.66 mm, 3.66 mm, and 4.66 mm were collected for the tissue-simulating phantoms with a scattering coefficient of 108 cm^{-1} and 222 cm^{-1}. Data was acquired from 500 to 700 nm (in 5 nm steps) with 1250 laser pulses averaged per wavelength. For tissue simulating phantoms with higher scattering coefficients, the PMT high-voltage was decreased for WTM measurement. The data acquisition time for each tissue-simulating phantom (see Section 5.2.1) was 49 seconds. As discussed in Section 5, this time can be substantially reduced with straightforward modifications, by decreasing the number of laser pulses averaged, or increasing the step size.

Figure 6(a) shows steady-state fluorescence spectra for each phantom, averaged over three sites and normalized to the area under the curve. Each of these spectra is a combination of the fluorescence spectra of gelatin (dark red curve) and Rhodamine B (dark green curve). The spectra of the four phantoms are very similar, with some small variations around 515 nm and 575 nm, where the standard deviations (error bars) are also higher. These variations may be the result of a variable gelatin fluorescence signal in the phantoms. Figure 6(b) plots time-resolved fluorescence decay curves obtained from averaging measurements at peak intensity

#130228 - $15.00 USD Received 16 Jun 2010; revised 6 Aug 2010; accepted 7 Aug 2010; published 10 Aug 2010
(C) 2010 OSA

at the three sites on each phantom. The small standard deviations (error bars) show that the decays at all three sites are similar.

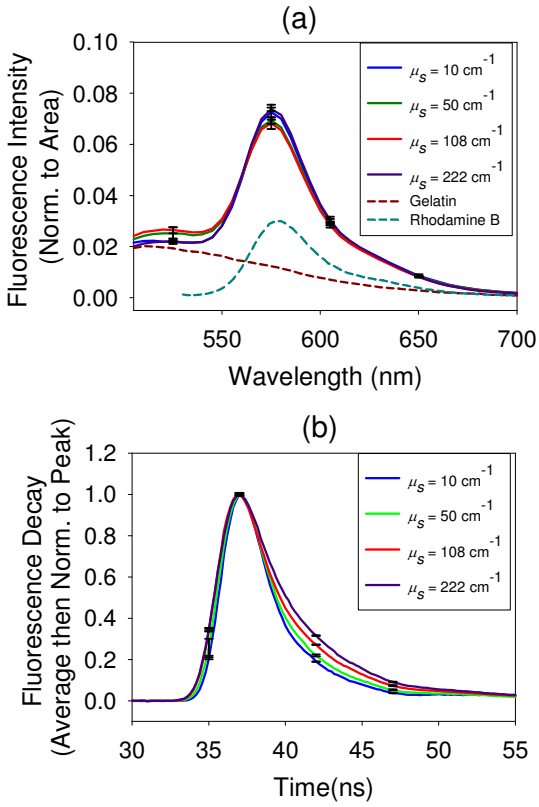

Fig. 6. Wavelength-resolved (a) and time-resolved (b) fluorescence from tissue-simulating phantoms with varying scattering coefficients (measured with a source detector separation of 0.66 mm). Three sites on each phantom were measured. The spectra represent the average of the three sites, with error bars representing standard deviation. Panel (a) also includes spectra from pure gelatin and from a solution of rhodamine B in deionized water.

Figure 6(b) suggests that phantoms with increased scattering coefficients exhibited stretched waveform decay. The stretched waveform decay shown in Fig. 6(b) for tissue-simulating phantoms with a μ_s of 108 cm^{-1} and 222 cm^{-1} (using a fiber-probe source-detector separation of 660 μm) was also observed for larger source detector separations out to 4.66 mm (data not shown). The distortion of the waveform was observed for each source-detector separation measured, with the relative waveform differences between each phantom remaining the same. For the 4.66 mm source-detector separation, at which the diffusion approximation is valid, the experimentally observed trend matched the prediction of diffusion theory (Fig. 7) [1]. In Fig. 7, the experimental results and the diffusion theory predictions were both time-shifted to align the rising shoulders of the decay curves for the two different scattering coefficients (108 cm^{-1} and 222 cm^{-1}). Additionally, both diffusion theory results were convolved with the corresponding instrument response functions from the phantom measurements. Computational studies employing Monte Carlo codes to model photon propagation are underway to further investigate the effect of increased optical scattering coefficients on the resulting transient fluorescence decay and extracted fluorophore lifetime [16,31,32].

#130228 - $15.00 USD Received 16 Jun 2010; revised 6 Aug 2010; accepted 7 Aug 2010; published 10 Aug 2010
(C) 2010 OSA

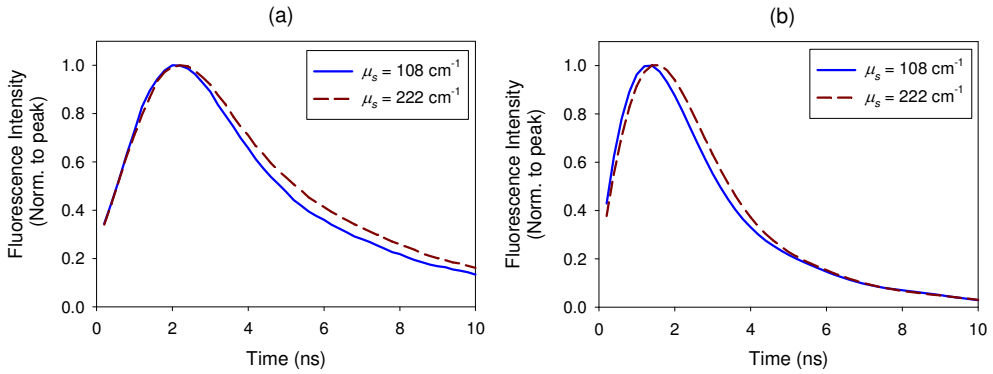

Fig. 7. Measured time-resolved fluorescence decay curves from two phantoms with biologically-relevant scattering coefficients at a source-detector separation of 4.66 mm (a), compared with the predictions of diffusion theory (b). Each curve in (b) is a convolution of the diffusion theory result with the instrument response function of the corresponding tissue-simulating phantom. For the sake of comparison, the experimental results and the diffusion theory predictions were time-shifted to align the rising shoulders of the curves. In both panels, the time-resolved decay from the medium with the higher scattering coefficient (red dashed curve) was noticeably broader than the decay from the medium with the lower scattering coefficient (blue solid curve).

5. Discussion

Most clinical fluorescence instruments emphasize the spectral domain, often integrating a spectrograph and CCD camera for rapid data collection in which the entire spectrum is measured at once. In these systems, data is acquired over multiple laser shots for signal averaging. Most approaches for acquiring time-resolved fluorescence employ a pulsed laser and digital oscilloscope. The nitrogen laser is often employed because it is small, relatively low cost, and its UV wavelength (337 nm) excites endogenous fluorescence. However, the effectiveness of the nitrogen laser for rapid collection of time-resolved fluorescence is hindered by its relative low pulse repetition frequency.

In this report, we employed a 473 nm microchip laser (3 kHz repetition rate) and a specialized digitizer capable of collecting the data obtained at this rate. The system was tested on standard fluorophore solutions and tissue-simulating phantoms. WTMs from samples with fluorophore concentrations of 1 μM were acquired with speed (under 25 s for a WTM from 500 to 650 nm with a 5 nm step size and 125 laser pulses averaged) and precision (error less than 1% for Rhodamine 6G and Fluorescein solutions), without maximizing the sensing capabilities of the transient digitizer.

The autofluorescence intensity measured from biological tissues depends on several factors, including the excitation wavelength, fiber-probe geometry, and composition of the biological sample. It is likely that detected autofluorescence signals from biological tissues will be weaker than those from the stock fluorescent solutions used in this study. To compensate for this signal loss, system parameters can be changed to increase the detected fluorescence intensity. For example, the excitation fiber diameter can be increased in size to excite a larger sample volume and the detection fiber diameter can be increased to detect a larger portion of the emitted fluorescence photons. In addition, the PMT gain can be increased in order to maximize the dynamic measurement range of the digitizer.

We note that the stretched behavior of the fluorescence decay curves from phantoms with increased scattering coefficients is under investigation. Preliminary results suggest that the Rhodamine B lifetime in the phantom is different than its value in cuvette solution, which may be due to the dependence of the fluorescence properties of Rhodamine B on its local environment [30]. Specifically, the lifetime of Rhodamine B within the phantoms may have

#130228 - $15.00 USD Received 16 Jun 2010; revised 6 Aug 2010; accepted 7 Aug 2010; published 10 Aug 2010
(C) 2010 OSA

been altered by the presence of the gelatin and microspheres. Studies are underway employing phantoms containing a more stable fluorophore (Rhodamine 6G [30]).

It is important to note that the system set-ups reported here were designed only for point measurements, not imaging. However, the system can be modified to perform scans of multiple points on a sample in order to generate spatially-resolved information. Spatial resolution can also be obtained by use of fiber-probes with multiple source-detector separations.

It is also important to note that the acquisition speed of this system is not fully optimized. Acquisition time depends on laser pulse repetition frequency, number of laser pulses averaged per waveform, and spectral resolution. In addition, there is the time overhead associated with moving from one wavelength to the next and downloading an averaged waveform. Much of the time needed to generate the WTM data presented in this report was consumed by data transfer to a computer and stepping of the monochromator. The actual time it takes for the stepper motor to advance to the next wavelength once the command has been received and recognized is very small. Likewise, the data transfer time is very fast once the computer is alerted that data is ready for transfer and the computer communicates that it is ready to receive this data. Additional delays are caused by having the computer update the graphical display after each waveform.

Currently, waveform averaging is performed on the digitizer and, one at a time, the averaged waveforms are downloaded. However, the digitizer can store up to 4000 waveforms before its memory is full. If 100 laser pulses were averaged per waveform (including the 5X interleaving), the data associated with 40 such waveforms (corresponding to the wavelength range from 500 nm to 695 nm in steps of 5 nm) could be packed in memory. For a laser pulse repetition rate of 4000 Hz, the 100 pulses necessary per waveform are generated every 25 ms. The monochromator could be independently controlled to step every 25 ms without any intermediate communication once the sequence is initiated. In this scenario, the operator could hit a keystroke (or depress a foot pedal) to start the acquisition, then after a brief delay the full WTM would be collected in one second. Data transfer from the digitizer memory to the computer would take a few additional seconds, after which the system would be ready to repeat the process. The actual waveform averaging could then be performed on the computer, post data collection.

6. Conclusions

In this paper, we reported on the design and validation of novel technology for rapid, precise, and accurate acquisition of fluorescence wavelength-time matrices (WTMs) from fluorophore solutions and tissue-simulating phantoms. The clinically compatible technology employs a microchip laser with a 3 kHz repetition rate and a digitizer capable of detecting at this rate. The system can rapidly acquire fluorescence WTMs with high signal-to-noise ratio (greater than 100 when averaging 125 laser pulses per emission wavelength). The compact size enables future system translation to a portable, clinically-compatible unit. Integrated fiber-optic probes to deliver excitation light and detect fluorescence emission provide the capability for remote sensing of fluorescence from biological tissues.

These results suggest that the system will be able to perform rapid and accurate measurements of time- and wavelength-resolved fluorescence in a biomedical environment. The accurate, rapid, and portable nature of the system, combined with the information-rich fluorescence data set supplied by WTM collection, suggest that the technology reported here is potentially useful for a number of biomedical optics applications in clinical settings.

Acknowledgements

The project was supported in part by National Institutes of Health grants R43-EB-007866 (to G. D. G. and M.-A. M.) and R01-CA-114542 (to M.-A. M.), and by the Montana Board of

Research and Commercialization Technology, grant 08-48 (to G. D. G.). We thank Kurt Peterson from Fluorescence Innovations for technical assistance.

#130228 - $15.00 USD Received 16 Jun 2010; revised 6 Aug 2010; accepted 7 Aug 2010; published 10 Aug 2010
(C) 2010 OSA